Modeling of Autothermal Catalytic Monolith Reformer to Obtain hydrogen for Fuel Cells (Considering the Effect of the Amount of Steam and the Inlet Gas Temperature)

Abstract

The modeling of an autothermal catalytic monolith reformer to obtain hydrogen for fuel cells (considering the effect of the amount of steam and the inlet gas temperature) was studied in this paper. For this purpose, a catalytic monolithic reformer, including the methane autothermal reforming process, was 3D modeled, and the catalyst used in the present modeling was 5% $Ru - \gamma\ Al_2O_3$. This modeling was based on the simultaneous solution of the conservation equations, in which the effect of performed reactions was also considered. One channel of this monolithic reactor was used as the computational domain. The results of this modeling agreed with the laboratory data available in the literature. This model was used to estimate the performance of the reformer in other operating conditions. The parameters studied in the present research were the inlet steam/methane molar ratio and the reformer inlet gas temperature. Finally, it was found that to reach the maximum hydrogen content in the range of operational parameters; the reactor inlet gas temperature must be equal to 600°C.

Keywords: *Fuel cells, Catalytic reformer, Hydrogen production, Steam, Gas temperature*

Farnaz Mahdavi Dehkharghani

Ph.D., Department of Energy and Environment, Shahid Beheshti University, Tehran Iran. Farnazmahdavi841@gmail.com

Introduction

Partial oxidation of the fuel is used to provide the heat required for the endothermic fuel reforming reactions in the autothermal reformer. Steam is also added to the inlet feed. The amount of net heat generated in the autothermal reforming process almost equals zero. The advantage of the autothermal reforming reaction is that higher hydrogen content is obtained through the steam reforming process than the partial oxidation reaction. On the other hand, due to the partial oxidation reaction, a lower inlet temperature is required for the inlet gas stream than the steam reforming process. Also, the amount of soot is reduced due to steam. Various kinetic models have been proposed for methane combustion, and some of these mechanisms are complex. Deutschmann et al. **[1]** developed a mechanism for the partial oxidation of methane using a Pt catalyst, which included 100 primary reactions and 30 chemical species. Modeling such a system is very expensive. Among these reactions, some reactions limit the reaction rate, and other reactions may be ignored. It can be seen that a simplified mechanism can accurately predict the concentration of products at the reactor outlet. De Groote and Froment **[2]** proposed a mechanism including 9 reactions to model methane reforming reactions. The model proposed by Akers et al. **[3]** is one of the first models presented about the Steam Methane Reforming (SMR) reaction. This model focused on the effect of concentration on the intensity of the reaction between steam and natural gas using a nickel catalyst (at a temperature of about between 340 and 640 °C and a pressure of 1 atm). The selected conditions were not thermodynamically suitable for carbon formation, and methane equilibrium conversion was also high. Numaguchi and Kikuchi **[4]** studied the steam methane reforming reaction using an 8.7% (wt.) Ni/Al_2O_3 catalyst.

In this study, the temperature was between 400 and 890 °C, the pressure was between 1.2 and 25.5 bar, and the inlet steam/methane molar ratio was between 1.44 and 4.5. Hou et al. **[5]** kinetically studied the steam methane reforming reaction and water-gas shift reaction using a commercial Ni/α-Al_2O_3 catalyst under unlimited diffusion conditions. According to the results of their study, surface reactions between adsorbed particles were the controlling step in steam reforming. D.L. Hoang et al. **[6]** used the intensity equation Xu, and Froment proposed in their kinetics study and obtained the corresponding kinetic coefficients through experiments for the used catalyst (NiS/α-Al_2O_3). Barrio et al. **[7]** also used the kinetics model Xu, and Froment presented and obtained its coefficients for a 5% $Ru - \gamma\ Al_2O_3$ catalyst. Trimm and Lam **[8]** obtained a rate equation for the complete combustion of methane based on a Pt/Al_2O_3 catalyst at a high temperature of 557°C and an O_2/CH_4 molar ratio between 0.3 and 5. Ma et al. **[9]** studied methane, ethane, and propane oxidation kinetics using a Pt catalyst. They obtained two relationships to describe the kinetics of methane oxidation. Kinetical expressions have been obtained for temperatures of 360-460 °C. Wheeler et al. **[10]** investigated the water-gas shift reaction on active metals (such as Pt, Rh, and Ru) and other metals (such as Ni and Pd) with CeO_2 at short contact times (0.008-0.05 s) and temperatures of 300-1000 °C. They concluded that a simple rate equation provides a good fit for the data at all temperatures

(from the equilibrium conversion percentage to the low conversion percentage). According to the mentioned cases, the current research aims to model an autothermal catalytic monolith reformer to obtain hydrogen for fuel cells (considering the effect of the amount of steam and the inlet gas temperature).

Characteristics of modeled monolithic reactor

Rabe et al. **[11]** used a monolithic reactor equipped with a thermocouple (TC) to record the temperature throughout the reactor. There was a plate for better mixing of gases in the initial zone of this reactor and before the first monolithic zone. This plate provided a laminar flow to pass through the monolithic zone. Also, there were three monolithic zones, in which only one zone used a catalyst, and the other two were without a catalyst. The catalyst used in the present laboratory work was 5% $Ru-\gamma\,Al_2O_3$. They also studied the effect of two catalytic monolith zones and concluded that the presence of a second catalytic zone has no significant effect on the reactor performance. The diameter and length of each monolithic zone were 3.5 cm. The number of channels of a monolithic reactor is usually defined as the number of cells per square inch (cpsi), which was 400 cpsi for the used reactor, and there were about 597 channels considering the diameter of the monolith reactor. Water was pumped into an evaporator, mixing the steam with methane. The steam/methane mixture was preheated to 275 °C, and oxygen entered the reactor at room temperature. To start the test, the reactor was heated up to the catalytic combustion temperature of the inlet feed (about 500 °C) by a heater, and external heating of the reactor was stopped after the combustion reaction. Figure 1 shows a view of this reactor.

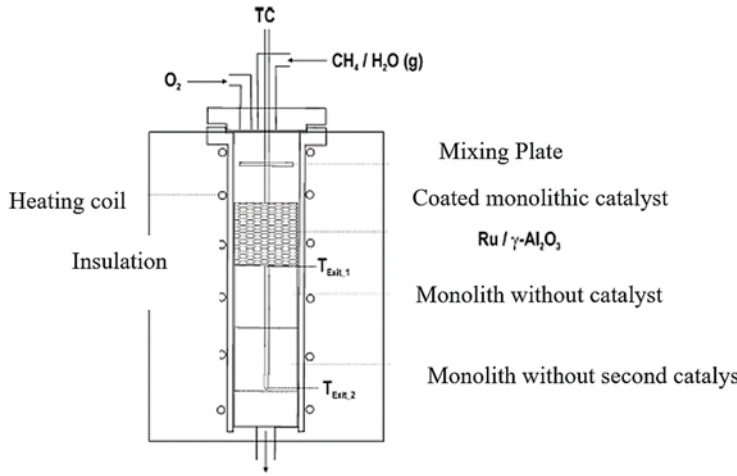

Fig. 1. Reactor used by Rabe **[11]**

Modeling the entire reactor is very expensive and time-consuming. Thus, it is assumed that the behavior of all channels is the same and similar to the behavior of the entire reactor, so only one channel of this reactor was modeled. The channels of this monolithic reactor were considered cylindrical; therefore, the symmetry of this type of channel was beneficial, and only one-quarter of the channel was needed to model. The diameter of each monolithic channel used by Rabe **[11]** was 0.9 mm, and its length was 3.5 cm for each monolithic zone. The initial mixing zone was omitted to model this set, and it was assumed that the gas mixture entering the first monolithic zone was completely homogeneous. According to the assumption, only three monolithic zones were considered in the modeling, equivalent to a length of 10.5 cm. Since the length/diameter ratio of the channel was much higher, only a part of the meshed surface of the used geometry is given in Fig. (2).

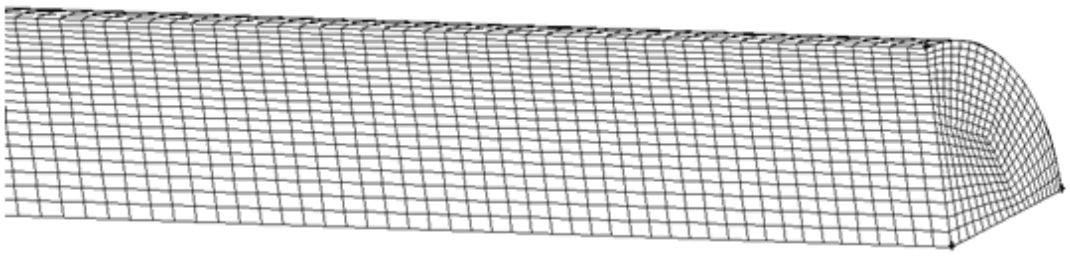

Fig. 2. The meshed surface of the geometry used in modeling

There were about 37500 meshes on the volume. Since the temperature and species concentration changes at the reactor inlet are fast, the number of meshes considered at the beginning of the reactor was more.

Assumptions and equations used in modeling

According to the laboratory results of Rabe et al. **[11],** when the Weight Hourly Space Velocity (WHSV) (the ratio of the reactant mass fed to the reactor per hour to the catalyst mass, 3.1 g 5% Ru-γAl_2O_3 per monolith) is equal to 119 hr^{-1}, the R_e number in the channel of the used monolithic reactor will be

equal to 32, indicating that the flow in the channel is laminar. The fluid flow inside the channel and the gas mixture were assumed incompressible and ideal, respectively. Since the operating pressure inside the reactor was 2/1 bar and the pressure drop in the monolithic reactor was very small, these assumptions were reasonable. The modeling of this system was performed in a steady state. The equations of continuity, momentum, energy, and chemical species considered were as follows **[12].** In the following, the methods of calculating the parameters of these equations are presented, adapted from the literature **[12].** These equations were solved using FLUENT 6.3.26 software.

$$\frac{\partial uj}{\partial x_j} = 0$$

(1)

$$\rho.u_j \frac{\partial u_i}{\partial x_j} = -\frac{\partial p}{\partial x_i} + \frac{\partial \tau_{ij}}{\partial x_j} + \rho g_i$$

(2)

$$\rho.u_j \frac{\partial h}{\partial x_j} = \frac{\partial}{\partial x_j}(k_{eff} \frac{\partial T}{\partial x_j} - \sum_{i=1}^{N} h_i J_{ij}) + u_j \frac{\partial p}{\partial x_j} + S_h$$

(3)

$$\rho.u_j \frac{\partial Y}{\partial x_j} = -\frac{\partial J_{ij}}{\partial x_j} + R_i$$

(4)

Where u (m/s) is gas velocity, ρ (kg/m^3), gas density, p (Pa), static pressure, τ_{ij} (Pa), laminar flow stress tensor, ρg (N/m^3), gravitational body force per unit volume, h (kJ/kg), enthalpy, K_{eff} (W/m.K), the effective thermal conductivity (ETC), T (K), the temperature of the gas mixture, h_i (kJ/kg), the enthalpy of specie i, and J_{ij} (kg/m^{2}s), the diffusive flux of specie i in the j-direction, which is assumed to include the full multicomponent diffusion and heat-induced diffusion. N is the total number of gas species, S_h, is the energy source resulting from the chemical reaction (kW/m^3), Y_i, the local mass percent combination of the species, and R_i (kg/m^3.s), is the net production rate of specie i by chemical reaction. The stress tensor of laminar flow (τ_{ij}) is obtained from the following equation:

$$\tau_{ij} = \mu(\frac{\partial u_i}{\partial x_j} + \frac{\partial u_j}{\partial x_i} - \frac{2}{3}\frac{\partial u_l}{\partial x_l}\delta_{ij})$$

(5)

Where μ (N.s/m^2) is viscosity. The first two terms on the right of the energy equation (Eq. 3) are the energy transferred due to thermal conduction and species diffusion. The thermal energy produced by the viscous shear effect in the flow is neglected. The effective thermal conductivity for the fluid flow in a channel is similar to fluid thermal conductivity, and for the fluid flow in a porous medium is obtained from the following equation:

$$Keff = \varepsilon K_f + (1-\varepsilon)K_s$$

(6)

Where ε is the substrate porosity coefficient, K_f, is the thermal conductivity of the fluid, and K_s is the thermal conductivity of the solid material. Enthalpy, h (kJ/kg), for an ideal gas mixture, is defined as follows:

$$h = \sum_{i}^{N} Y_i h_i$$

(7)

Furthermore, h_i is obtained as follows:

$$h_i = \int_{T_{ref}}^{T} C_{p,i} dT$$

(8)

Where $C_{p,i}$ (kJ/kg.K) is the specific heat of the specie, i and T_{ref} are the reference temperature (T_{ref} in the present research was 298.15 K). The term of the energy source, S_h (kW/m^3), is calculated from the following equation:

$$S_h = -\sum_{i} \frac{h_i^{\circ}}{M_{w,i}} R_i$$

(9)

Where h_i° (kJ/mol) is the formation enthalpy of specie i and $M_{w,i}$ (kg/mol) is the molecular weight of specie i. Since the molecular diffusion process is important in the fuel reformer, the diffusive flux of specie i, J_{ij}, is calculated using the full multicomponent diffusion method based on the Maxwell-Stefan equation:

$$J_{ij} = -\sum_{k=1,\neq i}^{N} \rho D_{ik} \frac{\partial Y_k}{\partial x_j} - D_{T,i} \frac{1}{T} \frac{\partial T}{\partial x_j}$$

(10)

Where $D_{T,i}$ is the thermal diffusion coefficient for specie i in the mixture and $D_{i,k}$ is defined as follows:

$$D_{i,k} = [D] = [A]^{-1}[B]$$

(11)

$$A_{ii} = -(\frac{X_i}{d_{iN}} \frac{M_w}{M_{w,N}} + \sum_{k=1,\neq i}^{N} \frac{X_k}{d_{ik}} \frac{M_w}{M_{w,i}})$$

(12)

$$A_{ik} = X_i\left(\frac{1}{d_{ik}}\frac{M_w}{M_{w,k}} - \frac{1}{d_{iN}}\frac{M_w}{M_{w,N}}\right)$$

(13)

$$B_{ii} = -\left(X_i\frac{M_w}{M_{w,N}} + (1-X_i)\frac{M_w}{M_{w,i}}\right)$$

(14)

$$B_{ik} = X_i\left(\frac{M_w}{M_{w,k}} - \frac{M_w}{M_{w,N}}\right)$$

(15)

Where [A], [B], and [D] are matrices with a size of (N-1)×(N-1). X_i is the mole fraction of specie i, M_w, the molecular weight of the mixture, $M_{w,N}$, the molecular weight of specie N, and $d_{i,k,}$ the binary mass diffusion coefficient for specie i in specie k. The thermal diffusion coefficient is calculated from the following equation:

$$D_{T,i} = -2.59\times10^{-7}\,T^{0.659}\left[\frac{M_{w,i}^{0.511}X_i}{\sum_{i=1}^{N}M_{w,i}^{0.511}X_i} - Y_i\right]\left[\frac{\sum_{i=1}^{N}M_{w,i}^{0.511}X_i}{\sum_{i=1}^{N}M_{w,i}^{0.489}X_i}\right]$$

(16)

The binary mass diffusion coefficient is calculated using the Chapman-Enskog equation. This relationship is as follows:

$$d_{ik} = 0.00188\frac{\left[T^3\left(\frac{1}{M_{w,i}}+\frac{1}{M_{w,k}}\right)\right]^{0.5}}{p_{abs}.\sigma_{ik}^2\Omega_D}$$

(17)

Where P_{abs} is the absolute pressure, the Lennard-Jones (LJ) effective diameter for impact Ω_D is diffusion collision integral. σ_{ik} is calculated as follows for a binary mixture:

$$\sigma_{ik} = 0.5\,(\sigma_i + \sigma_k)$$

(18)

Ω_D is obtained from the following equation:

$$\Omega_D = f(T_D^*) = f\left(\frac{T}{(\varepsilon/k_B)_{ik}}\right)$$

(19)

Where $(\varepsilon/k_B)_{ik}$ is calculated for the mixture from the following equation:

$$(\varepsilon/k_B)_{ik} = \sqrt{(\varepsilon/k_B)_i.(\varepsilon/k_B)_k}$$

(20)

Where k_B is the Boltzmann constant.

The density of the gas mixture follows the ideal gas law, which is given below:

$$\rho = \frac{P_{op}M_w}{RT}$$

(21)

Where P_{op} (Pa) is the operating pressure.

It is assumed that the thermal conductivity and specific heat of any chemical specie i is a function of temperature, and this temperature equation is a polynomial:

$$\Phi_i = \sum_{k=1}^{m} C_k\,T^{\,k-1}$$

(22)

Where Φ_i thermal conductivity can be assumed or specific heat. The unit of temperature in this relation is (K). The thermal conductivity and specific heat of the gas mixture are calculated from the following equation:

$$\Phi = \sum_{i=1}^{N} Y_i\,\Phi_i$$

(23)

Modeling the reaction mechanism

Since solid and site species are usually very small, they are not considered in modeling the reaction mechanism. The r-th reaction on the wall, which includes only gaseous species, can be written as follows:

$$\sum_{i=1}^{N} g_{i,r}^{'}G_i \leftrightarrow \sum_{i=1}^{N} g_{i,r}^{''}G_i$$

(24)

Where G_i represents the gaseous specie, $g_{i,r}^{'}$, the stoichiometric coefficient for any reactant i, and $g_{i,r}^{''}$, the stoichiometric coefficient for any product i, the reaction mechanism includes a set of reactions that the above equation applies to all these reactions in the system. The coefficient of species that do not participate in the reaction equals zero. The net rate of production and consumption rate of any specie I, Ri ($kmol/m^2.s$), is obtained from the following equation:

$$\hat{R}_i = \sum_{k=1}^{N_{rxn}}(g_{i,r}^{''} - g_{i,r}^{'})r_k \qquad i = 1,2,3,...,N$$

(25)

Where N_{rxn} is the total number of reactions and r_k is the rate of the k-th reaction. Since the effect of gas phase reactions on the overall rate of reactions can be ignored, gas phase reactions are ignored in this modeling, and these reactions are considered only on the catalytic surface of the wall.

Kinetically relationships for methane autothermal reforming using Ru catalyst

For methane autothermal reforming, 6 chemical species, including CH_4, H_2O, O_2, H_2, CO, and CO_2, were considered in the modeling. The stoichiometry of the chemical reactions considered for methane autothermal reforming is equations (9)-(12). Since the amount of CO_2 is more than the amount of CO at the reactor outlet, to better estimate the amount of CO_2 at the reactor outlet, the autothermal reforming process was considered as a combination of the steam reforming process and complete combustion in this modeling. The rate equations provided by Xu and Froment **[13]** were used for the steam methane reforming process and the water-gas shift reaction, and the rate equations given by Ma **[9]** were used for the complete combustion of methane.

$$r_1 = \frac{k_1}{(1+K^1_{CH_4}p_{CH_4}+K^1_{O_2}\sqrt{p_{O_2}})^2}p_{CH_4}\sqrt{p_{O_2}}$$

(26)

$$r_2 = \frac{k_2}{p^{2.5}_{H_2}}\left(p_{CH_4}p_{H_2O}-\frac{p^3_{H_2}p_{CO}}{K^e_2}\right)\times\frac{1}{(DEN)^2}$$

(27)

$$r_3 = \frac{k_3}{p_{H_2}}\left(p_{CO}p_{H_2O}-\frac{p_{H_2}p_{CO_2}}{K^e_3}\right)\times\frac{1}{(DEN)^2}$$

(28)

$$r_4 = \frac{k_4}{p^{3.5}_{H_2}}\left(p_{CH_4}p^2_{H_2O}-\frac{p^4_{H_2}p_{CO_2}}{K^e_4}\right)\times\frac{1}{(DEN)^2}$$

(29)

Where DEN is defined as follows:

$$DEN = 1+K_{CO}p_{CO}+K_{H_2}p_{H_2}+K_{CH_4}p_{CH_4}+\frac{K_{H_2O}p_{H_2O}}{p_{H_2}}$$

(30)

The value of k_i in the expressions obtained by Xu and Froment at different temperatures is obtained through the Arenus equation, $k_i = A_i.\exp(-E_i/RT)$, where A_i is the pre-exponential factor, R represents the universal gas constant, and E_i stands for activation energy for the reaction. Kinetically data for different catalysts are given in the various literature. In the modeling, modified coefficients have been used for a 5% $Ru-\gamma Al_2O_3$ catalyst **[7].** These coefficients are presented in Table (1).

Table 1. Kinetically parameters for 5% $Ru-\gamma Al_2O_3$ catalyst (unit of activation energy is kJ/kmol) **[7]**

Reaction	Parameters of Ru catalyst	
1	A_1	5.6×10^{17} kmol.bar $^{-1.5}$/kg $_{cat}$.hr
	E_1	1.89×10^5
2	A_2	4.27×10^{15} kmol.bar $^{0.5}$/kg $_{cat}$.hr
	E_2	3.25×10^5
3	A_3	2.2×10^6 kmol.bar $^{-1}$/kg $_{cat}$.hr
	E_3	5.81×10^4
4	A_4	7.9×10^{14} kmol.bar $^{0.5}$/kg $_{cat}$.hr
	E_4	2.69×10^5

Also, adsorption coefficients (K_k) change with temperature as illustrated $K_k = A_k.\exp(-\Delta H_k/RT)$ so that k can be CH_4, O_2, H_2O, H_2, or CO. Adsorption coefficient constants for different materials in the reaction mechanism are presented in Table (2).

Table 2. Adsorption constants of materials for autothermal reforming process **[7]**

For r_1	For r_2, r_3, r_4

$A^{1}_{CH_4}$	$A^{1}_{O_2}$	A_{CH_4}	A_{H_2O}	A_{H_2}	A_{CO}
4.02×10^{5} bar $^{-1}$	5.08×10^{4} bar $^{-1}$	6.65×10^{-4} bar $^{-1}$	1.77×10^{5} bar $^{-1}$	6.12×10^{-9} bar $^{-1}$	8.23×10^{-5} bar $^{-1}$
103.5 kJ/mol	66.2 kJ/mol	-38.28 kJ/mol	88.68 kJ/mol	-82.90 kJ/mol	-70.65 kJ/mol

The relationship between reaction equilibrium constants with temperature is as $K_i^e = K_{Oi}.\exp(-H_i/T)$ that the constants of this relationship for steam reforming equilibrium reactions are presented in Table (3).

Table 3. Equilibrium constants for the authothermal reforming process **[7]**

	K_{Oi}	H_i
$K_2^e(bar^2)$	5.75×10^{12}	26285
K_3^e	1.26×10^{-2}	-4639
$K_4^e(bar^2)$	7.24×10^{10}	21646

In this paper, the constant equilibrium value for the second reaction at different temperatures was calculated with the help of thermodynamic relationships in reference **[14]** and compared with the constant equilibrium values obtained from Table (3) at the same temperatures. The relative error percentage for the equilibrium constant obtained from these two methods was less than 4%. As a result, H_i for the second reaction was considered equal to 26285 K in all simulations. The default rate equations in FLUENT software are as exponential relationships. Programming in C++ was used to consider methane autothermal reforming reactions using a 5% $Ru-\gamma Al_2O_3$ catalyst with non-Arrhenius rate equations. This program can be used for similar rate equations.

Results

The effect of the amount of inlet steam

To study the effect of the amount of inlet steam, in the first step, (i) H_2, CO, CO_2, and CH_4 concentration profiles along the reactor, (ii) methane conversion rate profile, (iii) temperature profile related to the state in where the H_2O/CH_4 ratio in the reactor inlet is 3.8 and the O_2/CH_4 ratio changes from 0.345 to 0.445 were provided and presented. The rest of the operating conditions were also according to the first condition of Table (1) (input thermal power is 1.09 kW). The flow rate of the inlet feed and the composition of the chemical species at the reactor inlet change corresponds to the ratio of O_2/CH_4 and H_2O/CH_4. Then, the effect of increasing steam at the inlet was investigated with the help of the "yield" quantity, which is introduced below. Figs. (3)-(6) show the concentration profile of H_2, CO, CO_2, and CH_4 along the reactor, and Fig. (7) shows the methane conversion rate for changing the O_2/CH_4 ratio from 0.345 to 0.445 in the H_2O/CH_4 ratio of 3/8. Fig. (8) shows the temperature profile related to these changes.

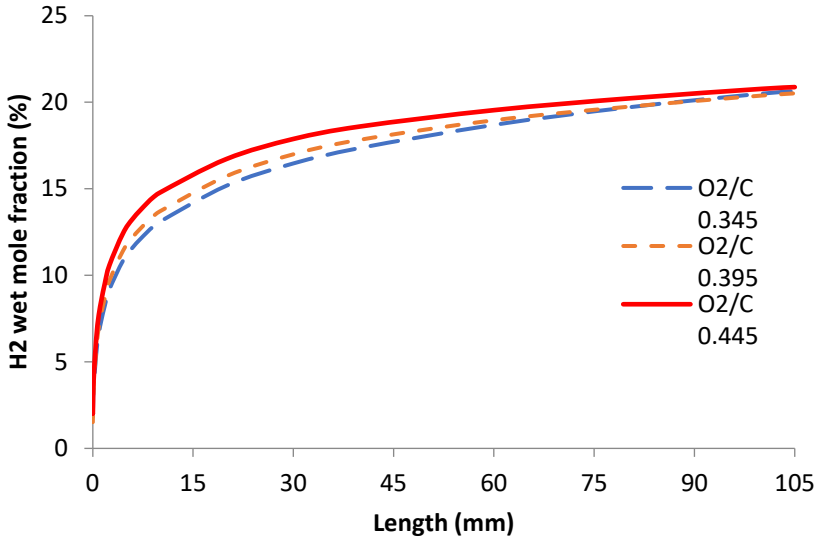

Fig. 3. Profile of hydrogen concentration vs. inlet oxygen content (H_2O/CH_4 = 3.8, and thermal power = 1.09 kW)

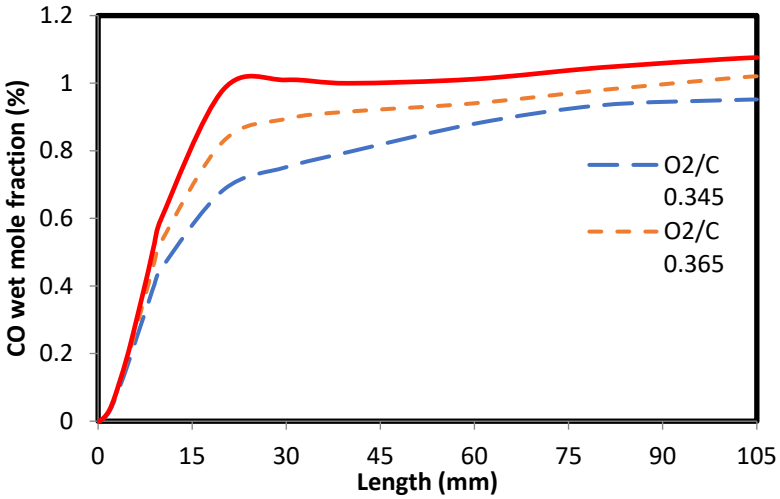

Fig. 4. Carbon monoxide concentration profile vs. inlet oxygen content (H_2O/CH_4 = 3.8, and thermal power = 1.09 kW)

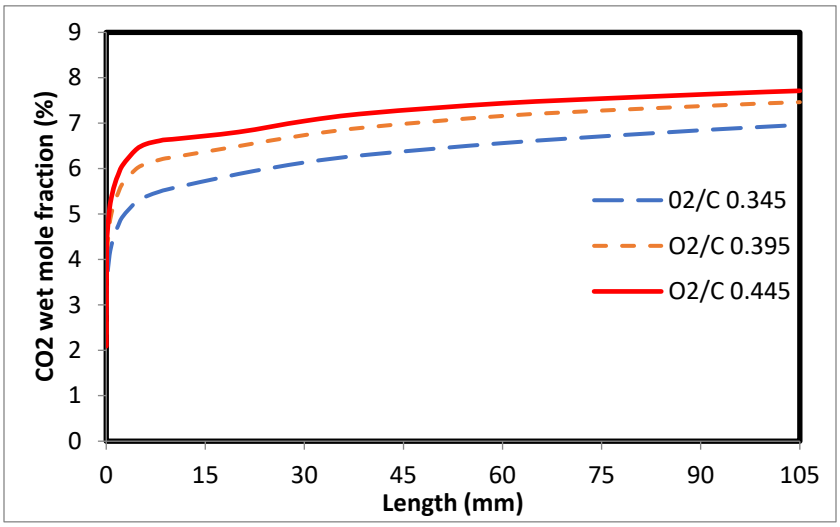

Fig. 5. Carbon dioxide concentration profile vs. inlet oxygen content (H_2O/CH_4 = 3.8, and thermal power = 1.09 kW)

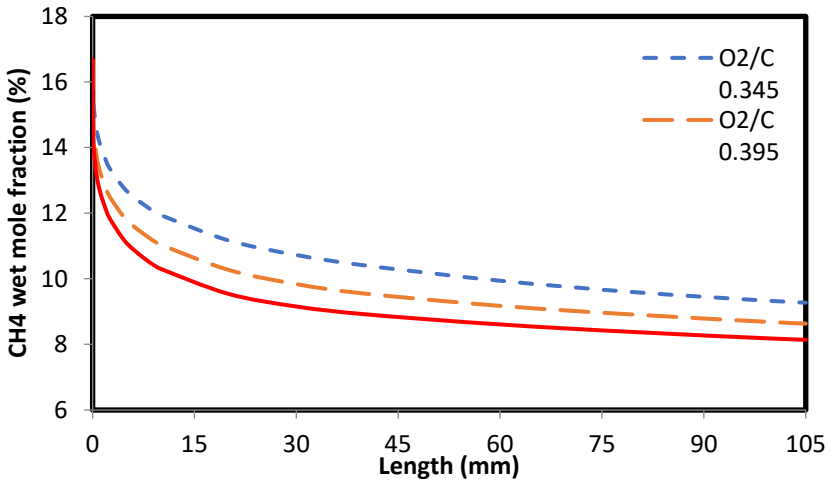

Fig. 6. Methane concentration profile vs. inlet oxygen content (H_2O/CH_4 = 3.8, and thermal power = 1.09 kW)

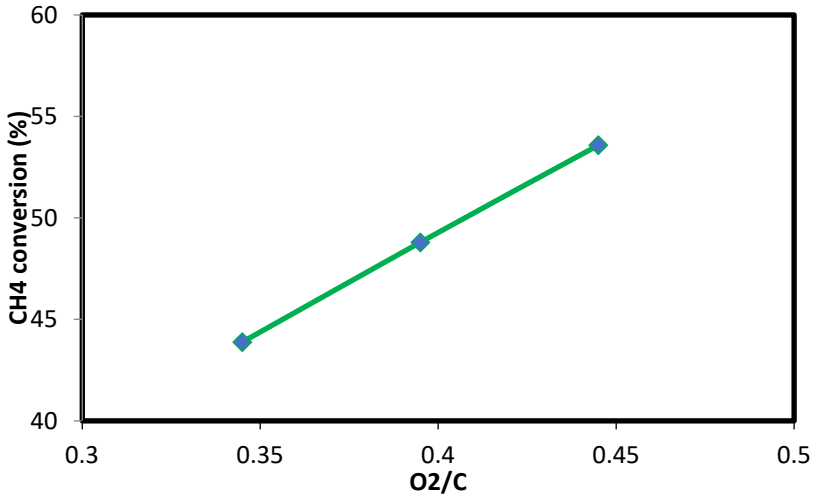

Fig. 7. The effect of inlet oxygen content on methane conversion rate (H_2O/CH_4 = 3.8, and thermal power = 1.09 kW)

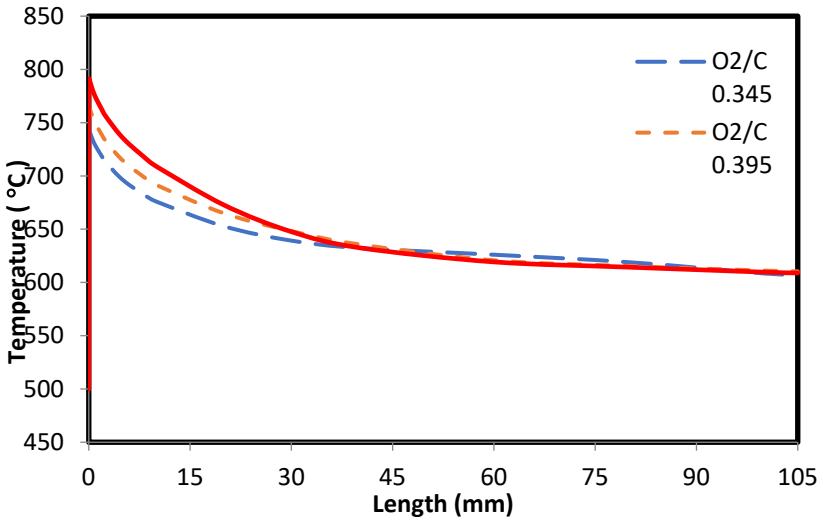

Fig. 8. Temperature profile vs. inlet oxygen content (H_2O/CH_4 = 3.8, and thermal power = 1.09 kW)

According to Figs. (3)-(8), the behavior of the concentration profiles of chemical species and the temperature inside the reactor does not change with the increase of the inlet steam, and it is similar to the behavior of the profiles in the condition where the H_2O/CH_4 ratio is equal to 2.9. A yield parameter is used to study the effect of increasing steam at the reactor inlet. For different chemical species, yield is defined as follows:

$$Y_{H_2} = \frac{H_{2out}}{3CH_{4in}} \quad (31)$$

$$Y_{CO} = \frac{CO_{out}}{CH_{4in}} \quad (32)$$

$$Y_{CO_2} = \frac{CO_{2out}}{CH_{4in}} \quad (33)$$

Tables (4)-(6) show the effect of increasing steam on hydrogen, carbon monoxide, and carbon dioxide yield.

Table 4. The effect of increasing steam on hydrogen yield (%)

	H_2O/CH_4 = 2.9	**H_2O/CH_4 =**3.8
O_2/C = 0.345	39.52	42.56
O_2/C = 0.395	40.60	41.14
O_2/C = 0.445	41.79	41.95

Table 5. The effect of increasing steam on carbon monoxide yield (%)

	H_2O/CH_4 = 2.9	**H_2O/CH_4 =**3.8
O_2/C = 0.345	6.92	5.88
O_2/C = 0.395	6.84	6.14
O_2/C = 0.445	8.50	6.45

Table 6. The effect of increasing steam on carbon dioxide yield (%)

	H_2O/CH_4 = 2.9	**H_2O/CH_4 =**3.8
O_2/C = 0.345	40.75	43.03
O_2/C = 0.395	41.79	44.89
O_2/C = 0.445	46.24	46.32

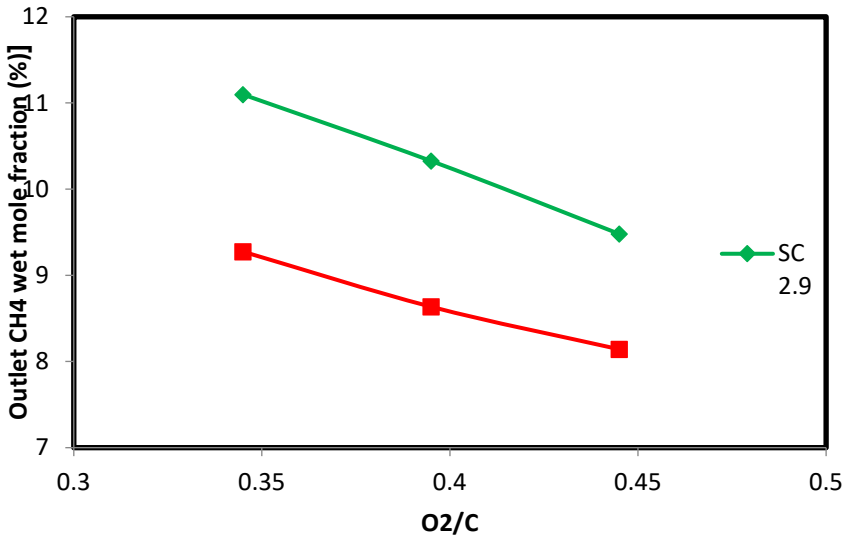

Fig. 9. The effect of the steam increase on the outlet methane wet mole fraction

As shown in Fig. (9), the amount of reactor outlet methane is lower (methane conversion rate is higher) at a higher ratio of H_2O/CH_4. On the other hand, the hydrogen yield is higher (Table 4) and the carbon monoxide yield is lower (Table 5) at a higher H_2O/CH_4 ratio. The operating temperature inside the reactor is also lower at a higher H_2O/CH_4 ratio (Fig. 9). The above cases can be discussed as follows: by increasing the ratio of H_2O/CH_4, the progress of reforming reactions with steam increases, and more methane is consumed, and as a result, the percentage of methane conversion increases. As a result of further progress in reforming reactions, the content of the produced hydrogen also increases. On the other hand, increasing the amount of inlet steam and the reforming reactions promote the water-gas shift reaction faster. However, the water-gas shift reaction is more sensitive to the increase of steam in the inlet. Due to the increase in the inlet steam, the rate of carbon monoxide consumption in the water-gas shift reaction will be higher than the reforming reaction production rate, and the amount of carbon monoxide in the reactor outlet will be lower. As mentioned, the increase of steam in the reactor inlet leads to faster progress of the reforming processes, and as a result, a decrease in temperature is observed at all points inside the reactor compared to the state where the inlet steam is less. However, adding more amounts of steam does not significantly affect reactor performance. The methane conversion rate increased slightly with the increasing H_2O/CH_4 ratio from 2.9 to 3.8.

.

Study the effect of inlet gas temperature

In this research, the inlet gas temperature was changed from 450 to 600 °C, and its effect on the outlet CH_4, H_2, and CO concentration and the temperature profile inside the reactor was investigated. The graphs related to these changes are presented in Figs. (10)-(13).

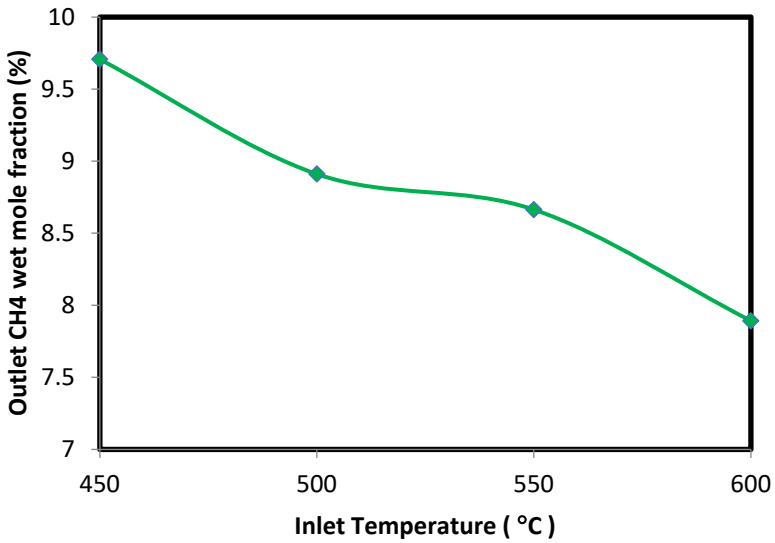

Fig. 10. The effect of inlet gas temperature on the outlet methane wet mole fraction

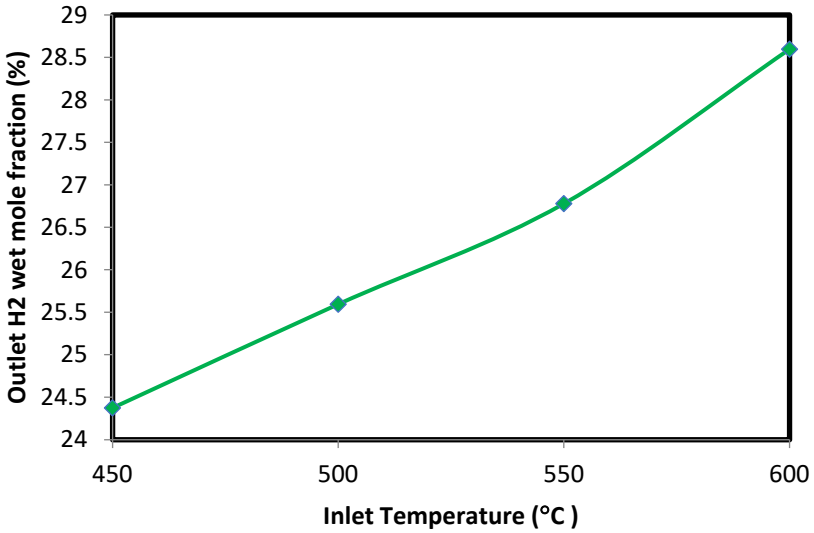

Fig. 11.
The effect of inlet gas temperature on the outlet hydrogen wet mole fraction

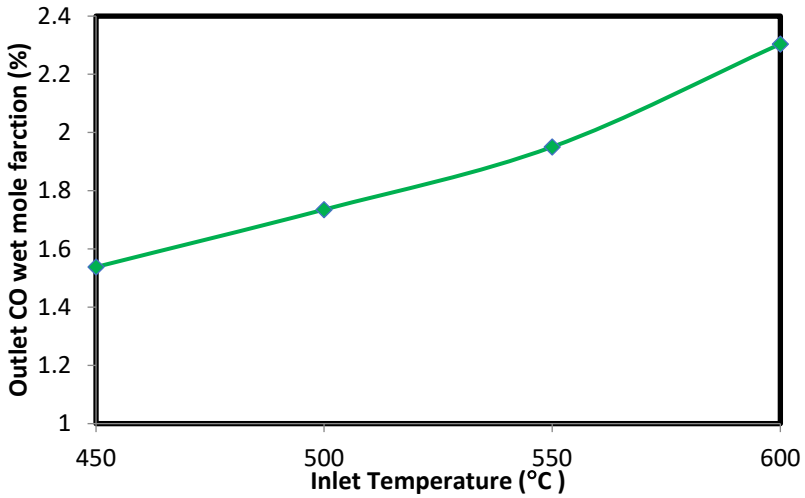

Fig. 12. The effect of inlet gas temperature on the outlet carbon monoxide wet mole fraction

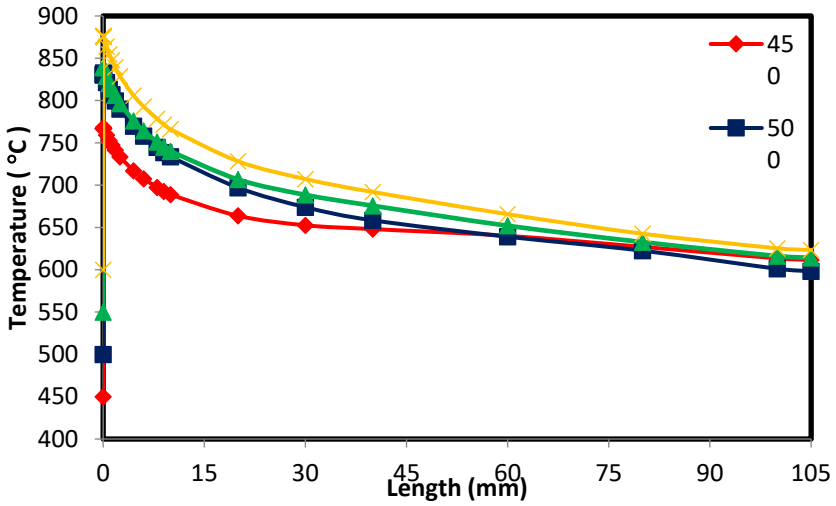

Fig. 13. The effect of inlet gas temperature on the temperature profile inside the reactor

According to Fig. (14), the reactor outlet methane concentration decreased with the increase in the temperature of the reactor inlet feed. This means that the percentage of methane conversion increases as the feed temperature increases. Also, the produced hydrogen and carbon monoxide content increased with the temperature of the reactor inlet gas. Because with the increase in the temperature of the reactor inlet gas, the rate of reforming reactions with steam increases, and as a result, the rate of hydrogen and carbon monoxide production increases. On the other hand, the exothermic nature of the water-gas shift reaction caused the higher temperature of the inlet gas to slow down its rate, and as a result, the increase of carbon monoxide in the temperature range of 450 to 600 °C is greater than the increase of hydrogen in this range. Also, by increasing the temperature of the inlet feed, the temperature inside the reactor and the temperature gradient at the beginning of the reactor increased. Figs. (14)-(17) show these four states' temperature contours along the reactor.

Fig. 14. The effect of a 450 °C temperature at the reactor inlet on the temperature contour inside it

Fig. 15. The effect of a 500 °C temperature at the reactor inlet on the temperature contour inside it

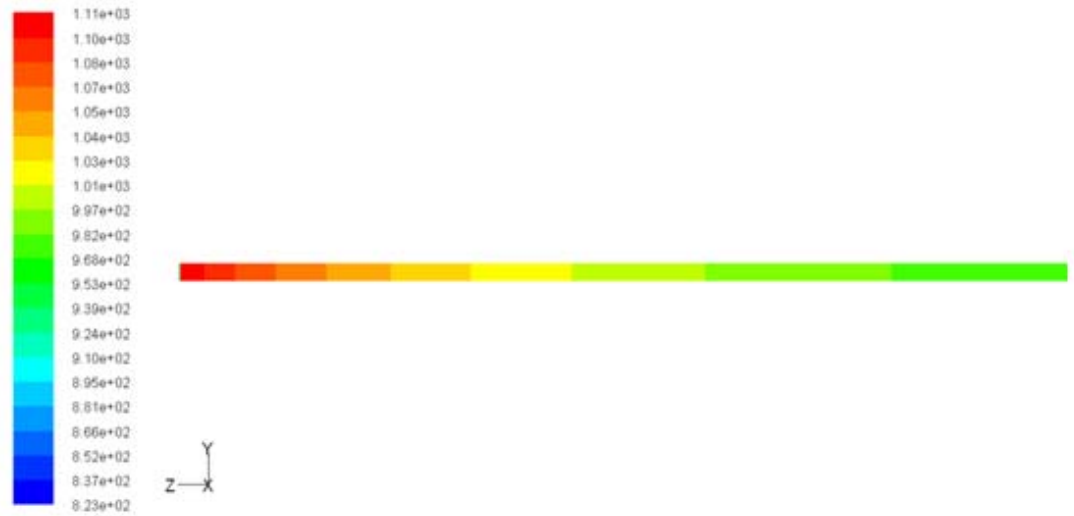

Fig. 16. The effect of a 550 °C temperature at the reactor inlet on the temperature contour inside it

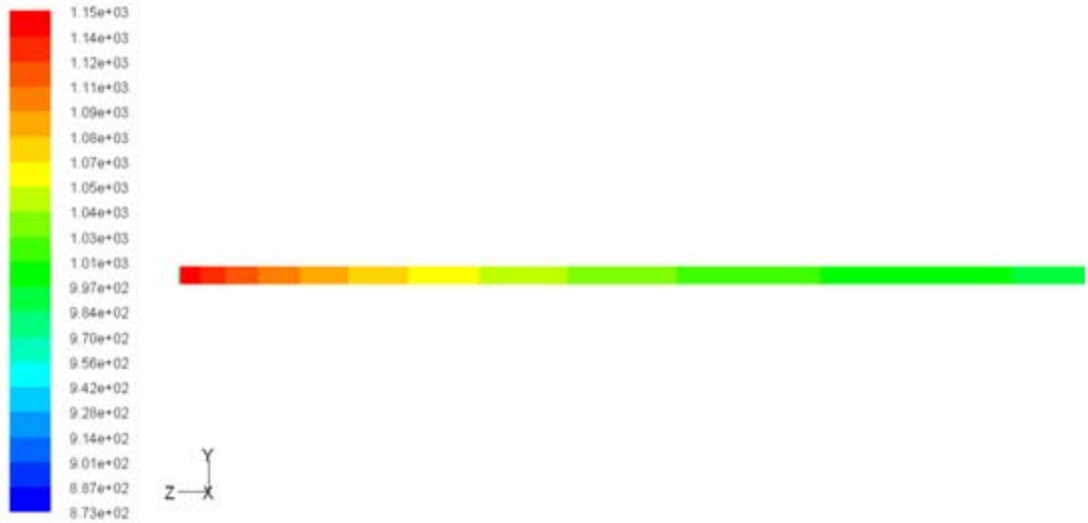

Fig. 17. The effect of a 600 °C temperature at the reactor inlet on the temperature contour inside it

As the temperature contours show, at a higher inlet temperature, the operating temperature inside the reactor increases at all points.

Conclusions

In the present research, a catalytic monolithic reformer, including the methane autothermal reforming process, was 3D modeled, and the catalyst used in the present modeling was 5% $Ru-\gamma\ Al_2O_3$. This modeling was based on the simultaneous solution of the conservation equations, in which the effect of performed reactions was also considered. One channel of this monolithic reactor was used as the computational domain. The results of this modeling agreed with the laboratory data available in the literature. This model was used to estimate the performance of the reformer in other operating conditions. The parameters studied in the present research were the inlet steam/methane molar ratio and the reformer inlet gas temperature. Finally, it was found that to reach the maximum hydrogen content in the range of operational parameters; the reactor inlet gas temperature must be equal to 600 °C. The innovation in the present research was the modeling of a 5% $Ru-\gamma\ Al_2O_3$ catalyst. In most of the modeling conducted in this research, separate industrial catalysts were used for the combustion and steam reforming processes. It should also be noted that a similar sample has not been observed for the 3D modeling of the methane autothermal reforming process using a 5% $Ru-\gamma\ Al_2O_3$ catalyst in a monolithic reactor.

Acknowledgments

None.

Conflict of interest

None.

Financial support

None.

Ethics statement

None.

……..

References

1. Deutschmann, O. Detailed Chemistry in CFD. Available at http://www.detchem.com/mechanisms/ (accessed August 28, 2007).
2. De Groote, A. M., Froment, G. F. (1996) “Simulation of the catalytic partial oxidation of methane to synthesis gas,” Applied Catalysis. A General, 138, 245-264.
3. Akers W. W., Camp D. P. (1955) “Kinetics of the methane-steam reaction,” AICHE J., Volume 1, No. 4, pp. 471-475.
4. Numaguchi T., Kikuchi K. (1988) “Intrinsic kinetics and design simulation in a complex reaction network, steam methane reforming,” Chem. Eng. Sci., Volume 43, No. 8, pp. 2295-2301.
5. Hou K., Hughes R. (2001) “The kinetics of methane steam reforming over a Ni/α-Al2O3 catalyst”, Chem. Eng. J., Volume 82, pp. 311-328.
6. Hoang D. L., Chan S. H., Ding O. L. (2005) “Kinetic and modeling study of methane steam reforming over sulfide nickel catalyst on a gamma alumina support,” Chem. Eng. J., Volume 112, pp. 1-11.
7. Barrio V. L., Schaub G., Rohde M., Rabe S. (2007) “Reactor modeling to simulate partial catalytic oxidation and steam reforming methane. Comparison of temperature profiles and strategies for hot spot minimization” International Journal of Hydrogen Energy 32, 1421–1428.
8. Trimm, D. L., Lam, C-W. (1980) “The combustion of methane on platinum-alumina fiber catalysts—I. Kinetics and mechanism,” Chemical Engineering Science, 35, 1405–1413.
9. Ma, L., Trimm, D. L., Jiang, C. (1996) “The design and testing of an autothermal reactor for the conversion of light hydrocarbons to hydrogen I. the kinetics of the catalytic oxidation of light hydrocarbons,” Applied catalysis. A: General, 138, 275-283.
10. Wheeler, C., Jhalani, A., Klein, E. J., Tummala, S., Schmidt, L. D. (2004), “The water–gas-shift reaction at short contact times.” Journal of Catalysis, 223, 191–199.
11. Rabe S., Truong T. B., Vogel F. (2007) “Catalytic autothermal reforming of methane: Performance of a kW scale reformer using pure oxygen as oxidant,” Applied Catalysis A: General, 318, 54–62.
12. Fluent, Inc. (2006). FLUENT 6.3 User's Guide. Lebanon, NH.
13. Xu J., Froment G. (1989) “Methane Steam Reforming, Methanation, and Water-Gas Shift: I. Intrinsic Kinetics,” AICHE J., Volume 35, No. 1, pp. 88-96.
14. P. M. Biesheuvel, G. J. Kramer “Two-Section Reactor Model for Autothermal Reforming of Methane to Synthesis Gas,” AIChE J. (2003), 49, 7.